Development of a Fluorescent-Tagged Kinase Assay System for the Detection and Characterization of Allosteric Kinase Inhibitors

7 AUTHORS, INCLUDING:

Jeffrey R Simard

Amgen

41 PUBLICATIONS **1,299** CITATIONS

SEE PROFILE

Vijaykumar Pawar

Florentis Pharmaceuticals Pvt. Ltd.

20 PUBLICATIONS **362** CITATIONS

SEE PROFILE

Development of a Fluorescent-Tagged Kinase Assay System for the Detection and Characterization of Allosteric Kinase Inhibitors

Jeffrey R. Simard, Matthäus Getlik, Christian Grütter, Vijaykumar Pawar,
Sabine Wulfert, Matthias Rabiller, and Daniel Rauh*

*Chemical Genomics Centre of the Max Planck Society, Otto-Hahn-Strasse 15,
D-44227 Dortmund, Germany*

Received March 15, 2009; E-mail: daniel.rauh@cgc.mpg.de

Abstract: Kinase disregulation disrupts the intricate network of intracellular signaling pathways and contributes to the onset of diseases such as cancer. Although several kinase inhibitors are on the market, inhibitor selectivity and drug resistance mutations persist as fundamental challenges in the development of effective long-term treatments. Chemical entities binding to less conserved allosteric sites would be expected to offer new opportunities for scaffold development. Because no high-throughput method was previously available, we developed a fluorescence-based kinase binding assay for identifying and characterizing ligands which stabilize the inactive kinase conformation. Here, we present a description of the development and validation of this assay using the serine/threonine kinase p38α. By covalently attaching fluorophores to the activation loop of the kinase, we were able to detect conformational changes and measure the K_d, k_{on}, and k_{off} associated with the binding and dissociation of ligands to the allosteric pocket. We report the SAR of a synthesized focused library of pyrazolourea derivatives, a scaffold known to bind with high affinity to the allosteric pocket of p38α. Additionally, we used protein X-ray crystallography together with our assay to examine the binding and dissociation kinetics to characterize potent quinazoline- and quinoline-based type II inhibitors, which also utilize this binding pocket in p38α. Last, we identified the b-Raf inhibitor sorafenib as a potent low nanomolar inhibitor of p38α and used protein X-ray crystallography to confirm a unique binding mode to the inactive kinase conformation.

1. Introduction

Aberrantly regulated kinases play causative roles in many disorders such as cancer, diabetes, neurological, immunological, and infectious diseases. Despite recent successes in kinase inhibitor drug discovery and the dawn of targeted tumor therapy, lack of inhibitor selectivity and efficacy, drug target validation, and the emergence of kinase drug resistance remain key challenges.[1] This can be attributed to the fact that most kinase inhibitors are ATP-competitive molecules, which form a critical hydrogen bond with the hinge region of the kinase domain (type I inhibitors) and often extend into the back of the ATP pocket in the vicinity of the gatekeeper residue, an amino acid situated at the back of the ATP pocket that is well-known for influencing type I inhibitor affinity and selectivity profiles among kinases.[2] Classical kinase inhibitors such as staurosporine and dasatinib are examples of type I inhibitors. The most common mutations occur at the gatekeeper position in the hinge region in which a small amino acid side chain (classically Thr) is exchanged for a larger hydrophobic residue (Ile or Met). Therefore, current medicinal chemistry endeavors seek to overcome these limitations by identifying new chemical entities that can bind "around" these mutations or bind to less conserved sites outside the ATP

pocket.[3,4] Such compounds would be expected to have improved selectivity profiles and offer new opportunities for scaffold development.[5] However, approaches that allow for the unambiguous identification of such inhibitors fall short.[6]

Kinases are typically found in the active, or DFG-in, conformation, which was first characterized in Protein Kinase A (PKA) with the activation loop open and extended, allowing ATP and substrate molecules to bind.[7] Structural changes in the activation loop, resulting from a 180° flip of the highly conserved DFG motif, result in an inactive, or DFG-out, conformation in which the Phe of the DFG motif obstructs ATP binding while exposing an adjacent allosteric site.[5,8] Type II inhibitors also bind to the hinge region and are ATP-competitive but take advantage of the DFG-out conformation by additionally extending into this allosteric site.[5] The structural transition associated with this event has been reported to increase the drug-

(1) Zhang, J.; Yang, P. L.; Gray, N. S. *Nat. Rev. Cancer* **2009**, *9*, 28–39.
(2) Apsel, B.; Blair, J. A.; Gonzalez, B.; Nazif, T. M.; Feldman, M. E.; Aizenstein, B.; Hoffman, R.; Williams, R. L.; Shokat, K. M.; Knight, Z. A. *Nat. Chem. Biol.* **2008**, *4*, 691–9.
(3) Backes, A. C.; Zech, B.; Felber, B.; Klebl, B.; Müller, G. *Expert Opin. Drug Discovery* **2008**, *3*, 1409–1425.
(4) Backes, A. C.; Zech, B.; Felber, B.; Klebl, B.; Müller, G. *Expert Opin. Drug Discovery* **2008**, *3*, 1427–1449.
(5) Liu, Y.; Gray, N. S. *Nat. Chem. Biol.* **2006**, *2*, 358–64.
(6) Annis, D. A.; Nazef, N.; Chuang, C. C.; Scott, M. P.; Nash, H. M. *J. Am. Chem. Soc.* **2004**, *126*, 15495–503.
(7) Knighton, D. R.; Zheng, J. H.; Ten Eyck, L. F.; Ashford, V. A.; Xuong, N. H.; Taylor, S. S.; Sowadski, J. M. *Science* **1991**, *253*, 407–14.
(8) Pargellis, C.; Tong, L.; Churchill, L.; Cirillo, P. F.; Gilmore, T.; Graham, A. G.; Grob, P. M.; Hickey, E. R.; Moss, N.; Pav, S.; Regan, J. *Nat. Struct. Biol.* **2002**, *9*, 268–72.

target residence time and provide efficacy at lower drug concentrations, thereby augmenting the therapeutic window.[9] The pyrazolourea BIRB-796, a selective inhibitor of p38α (developed by Boehringer−Ingelheim)[8,10,11] and imatinib (Gleevec), an Abl/cKit/PDGFR inhibitor,[12−14] are well-known examples of type II inhibitors. Additionally, a number of high affinity inhibitors that bind exclusively to the allosteric site of p38α are referred to as type III inhibitors. Such compounds also stabilize the DFG-out conformation and recently served as excellent starting points for the design and synthesis of type II inhibitors, which are able to overcome mutation-associated drug resistance in cSrc kinase.[15]

Considering the less-conserved nature of the amino acids lining the allosteric pocket, one would expect methods for discriminating between DFG-in and DFG-out binders to become valuable commodities to guide innovative compound design. Because insights into the stabilization of the DFG-out conformation by type II/III inhibitors were only demonstrated by protein X-ray crystallography nearly a decade ago with the development of imatinib,[14,16] currently available methods are few in number.[6,17] Additionally, there does not appear to be any high-throughput screening (HTS) method available, which can screen exclusively for DFG-out binders, that is rapid, robust, and easy to analyze. Therefore, we set out to develop a novel fluorescence-based kinase binding assay using p38α as a model for kinases regulated by the equilibrium between DFG-in and DFG-out conformations.

Here, we present our efforts to establish fluorescent-labeled p38α as a highly sensitive and reliable assay system for screening and identifying new DFG-out stabilizing scaffolds. More specifically, we describe how kinetic measurements such as k_{on} and k_{off} and direct measurements of K_d are achieved for DFG-out binders (types II and III) using this approach. Facilitated by this system, we were able to identify sorafenib as a high affinity binder of p38α and confirmed a unique type II inhibitor binding mode using protein X-ray crystallography, further highlighting the power of this approach for screening and discriminating compounds, which take advantage of the less-conserved allosteric binding pocket in some kinases.

2. Materials and Methods

2.1. Materials. The fluorophores *N*-((2-(iodoacetoxy)ethyl)-*N*-methyl)amino-7-nitrobenz-2-oxa-1,3-diazole (IANBD ester), 5-iodoacetamidofluorescein (5-IAF), *N*-(1-pyrene)iodoacetamide, 5-((((2-(iodoacetyl)amino)ethyl)amino)naphthalene-1-sulfonic acid (1,5-IAEDANS), and 6-acryloyl-2-dimethylaminonaphthalene (acrylodan) were purchased from Invitrogen GmbH (Karlsruhe, Ger-

many). Crystallization plates (EasyXtal Tool; 24-well) were obtained from Qiagen GmbH (Hilden, Germany). Cuvettes and mini stir bars were obtained from Carl Roth GmbH (Karlsruhe, Germany).

2.2. Protein Expression, Purification, and Labeling. The human p38α MAP kinase construct containing the mutations required for specific labeling (C119S/C162S/A172C) was cloned into a pOPINF vector and was transformed as an N-terminal His-tag construct with PreScission Protease cleavage site into BL21(DE3) *E. coli*. Cultures were grown at 37 °C until an OD600 of 0.6, cooled in 30 min to room temperature, and then induced with 1 mM IPTG for overnight (∼20 h) expression at 18 °C while shaking at 160 rpm. Cells were lysed in buffer A (50 mM Tris pH 8.0, 500 mM NaCl + 5% glycerol + 25 mM imidazole) and loaded onto a 30 mL Ni-column (self-packed), washed with 3 CV of Ni buffer A, and then eluted with a 0−50% linear gradient using Ni buffer B (Ni buffer A + 500 mM imidazole) over 2 CV. The protein was cleaved by incubating with PreScission Protease (50 μg/mL final concentration) in a 12−30 mL capacity 10k-MWCO dialysis cassette (Thermo Scientific) overnight at 4 °C in dialysis buffer (50 mM Tris pH 7.5, 5% glycerol, 150 mM NaCl, 1 mM EDTA, 1 mM DTT). The protein was then centrifuged for 15 min at ∼13 000 rpm to remove any precipitate that may have formed during the cleavage step. The supernatant was then taken and diluted 4-fold in anion buffer A (50 mM Tris pH 7.4, 5% glycerol, 50 mM NaCl, 1 mM DTT), loaded onto a 1 mL Sepharose Q FF column (GE Healthcare) and washed with 10 CV of anion buffer A. The protein was eluted with a 0−100% linear gradient of anion buffer B (anion buffer A + 600 mM NaCl) over 20 CV. The protein was pooled and concentrated down to 2 mL and passed through a Sephadex HiLoad 26/60 Superdex 75 column equilibrated with size exclusion buffer (20 mM Tris pH 7.4, 5% glycerol, 200 mM NaCl, 1 mM DTT) at a rate of 2 mL/min. The eluted protein was then concentrated to ∼10 mg/mL, aliquoted, and frozen at −80 °C.

Protein and a thiol-reactive fluorophore of choice (dissolved in DMF or DMSO) were combined in 20 mM HEPES buffer (pH 7.0) at a 1:1.5 ratio, respectively, and allowed to react in the dark overnight at 4 °C. The % v/v DMF was kept <0.5% during the conjugation. Conjugated protein was subsequently concentrated, washed three times in a 10k-MWCO Centricon using 50 mM HEPES (pH 7.45) + 200 mM NaCl, aliquoted, and frozen at −80 °C. Monolabeling of the protein was verified by ESI-MS and mass spectroscopic analysis of tryptic fragments (Figure S1).

2.3. Fluorescence Characterization of Fluorescent p38α Conjugates. Fluorophore-labeled p38α conjugates were excited at the known wavelength of each fluorophore, and emission spectra were recorded every 30 s in the absence and presence of saturating concentrations of BIRB-796 (DFG-out binder), to determine how the emission changes as the kinase shifts from the DFG-in to the DFG-out conformation. These measurements also revealed the most sensitive wavelength to monitor fluorescence changes in real-time (kinetics) and to assess the feasibility of using ratiometric fluorescence to plot binding curves (K_d). The emission spectra of each fluorescent−p38α conjugate (unbound and DFG-out saturated) were used to calculate the fluorescence parameters ΔI_{std} and ΔR_{max} as described elsewhere.[18] For most fluorophores, excitation and emission slits were set to 3 and 5 nm, respectively. In the case of pyrene, excitation and emission slits were set to 3 and 10 nm, respectively. For NBD, slits were set to 5 and 20 nm, respectively.

2.4. End Point and Kinetic Measurements. Fluorescent-labeled p38α (50 nM) and various concentrations of inhibitor (1 nM to 20 μM) were incubated in the dark at 4 °C overnight before end point fluorescence measurements were carried out in either polystyrene cuvettes or 96-well plates to determine the K_d of each compound. The same buffer that was used to wash and store the kinase was also used for all measurements. The long incubation times were

(9) Copeland, R. A.; Pompliano, D. L.; Meek, T. D. *Nat. Rev. Drug Discovery* **2006**, *5*, 730–9.
(10) Regan, J. *J. Med. Chem.* **2002**, *45*, 2994–3008.
(11) Regan, J.; Pargellis, C. A.; Cirillo, P. F.; Gilmore, T.; Hickey, E. R.; Peet, G. W.; Proto, A.; Swinamer, A.; Moss, N. *Bioorg. Med. Chem. Lett.* **2003**, *13*, 3101–4.
(12) Atwell, S. *J. Biol. Chem.* **2004**, *279*, 55827–32.
(13) Capdeville, R.; Buchdunger, E.; Zimmermann, J.; Matter, A. *Nat. Rev. Drug Discovery* **2002**, *1*, 493–502.
(14) Nagar, B.; Bornmann, W. G.; Pellicena, P.; Schindler, T.; Veach, D. R.; Miller, W. T.; Clarkson, B.; Kuriyan, J. *Cancer Res.* **2002**, *62*, 4236–43.
(15) Getlik, M.; Grütter, C.; Simard, J. R.; Klüter, S.; Rabiller, M.; Rode, H. B.; Robubi, A.; Rauh, D. *J. Med. Chem.* in press.
(16) Schindler, T.; Bornmann, W.; Pellicena, P.; Miller, W. T.; Clarkson, B.; Kuriyan, J. *Science* **2000**, *289*, 1938–42.
(17) Vogtherr, M.; Saxena, K.; Hoelder, S.; Grimme, S.; Betz, M.; Schieborr, U.; Pescatore, B.; Robin, M.; Delarbre, L.; Langer, T.; Wendt, K. U.; Schwalbe, H. *Angew. Chem., Int. Ed.* **2006**, *45*, 993–7.

(18) de Lorimier, R. M.; Smith, J. J.; Dwyer, M. A.; Looger, L. L.; Sali, K. M.; Paavola, C. D.; Rizk, S. S.; Sadigov, S.; Conrad, D. W.; Loew, L.; Hellinga, H. W. *Protein Sci.* **2002**, *11*, 2655–75.

required to avoid the K_d time dependence of type II inhibitors binding to p38α.[8] In the cuvette format, a series of cuvettes containing different amounts of inhibitor were prepared using inhibitor stocks (0.01, 0.1, 1.0, and 10.0 mM) prepared in DMSO. The % v/v DMSO did not exceed 0.2% in cuvettes. All measurements of the cuvettes were made with a JASCO FP-6500 fluorescence spectrophotometer (JASCO GmbH, Groβ-Umstadt, Germany). A Tecan Safire[2] (Tecan Deutschland GmbH, Crailsheim, Germany) was used to measure the fluorescence read-out in the 96-well plate format.

For acrylodan- and IAEDANS-labeled p38α, ratiometric fluorescence values enabled reliable binding curves to be plotted to directly determine the K_d of ligand binding to p38α. Where indicated, ratiometric fluorescence values obtained for unsaturated and p38α saturated in the DFG-out conformation were plotted as %p38α bound by the ligand. The %p38α bound is calculated as follows:

$$\% \text{ bound} = ((R - R_{\text{unsat}})/R_{\text{sat'd}}) \times 100$$

where R is the ratiometric fluorescence at a given concentration of ligand, and R_{unsat} and $R_{\text{sat'd}}$ are the ratiometric fluorescence values obtained for p38α in the absence or presence of a saturating concentration of the same ligand, respectively.

Rate constants for the association and dissociation of allosteric binders from p38α were determined using the cuvette format while monitoring fluorescence changes in real-time. A mini stir bar was placed in the bottom of each cuvette to ensure rapid mixing as inhibitor was delivered through the injection port located above the cuvette. The dissociation rate of allosteric binders was measured by adding a 10-fold excess of unlabeled p38α to a suspension of fluorophore-labeled p38α (0.1 μM) complexed with an equimolar amount of inhibitor while monitoring the fluorescence in real-time. The addition of excess unlabeled kinase causes the inhibitor to redistribute, resulting in a net dissociation of inhibitor from labeled-p38α, which is representative of the true k_{off} of the ligand.[19] The association rate of allosteric binders was measured by delivering increasing molar equivalents of compound (1−4:1 compound: protein), as demonstrated elsewhere,[19] to a suspension of fluorophore-labeled p38α (0.1 μM) while monitoring fluorescence changes in real-time. In the case of both association and dissociation, fluorescence changes were fit to a first-order function. The observed rate constant (k_{obs}) of the fluorescence change for the binding of a specific dose of compound was plotted against the inhibitor concentration, and the result is a straight line, which was fit linearly ($R^2 > 0.99$) with a slope equal to the k_{on} of that particular ligand. For all fluorescent p38α conjugates, association and dissociation rate constants could be used to calculate the equilibrium constant (K_{eq}) for the binding and dissociation of 100 nM BIRB-796 ($K_{\text{eq}} = k_{\text{off}}/k_{\text{on}}$).

2.5. ATP K_m and IC$_{50}$ Determination with an in Vitro Activity-Based Assay. IC$_{50}$ determinations for p38α kinase were measured with the HTRF KinEASE assay from Cisbio according to the manufacturer's instructions in which a GST-tagged ATF-2 peptide was phosphorylated by p38α. After completion of the reaction, an anti[phospho-ATF-2] antibody labeled with Europium Cryptate and an anti-GST antibody labeled with the fluorophore D2 were added. The FRET between Europium Cryptate and D2 was measured to quantify the phosphorylation of ATF-2. ATP concentrations were set at the K_m value for wild type, mutated/unlabeled, and the mutated/labeled p38α. Kinase and inhibitor were preincubated for 2 h before the reaction was started by addition of ATP and ATF-2. A Tecan Safire[2] plate reader was used to measure the fluorescence of the samples at 620 nm (Eu-labeled antibody) and 665 nm (D2-labeled antibody) 60 μs after excitation at 317 nm. The quotient of both intensities for reactions made with eight

different inhibitor concentrations was fit to a Hill four-parameter equation to determine IC$_{50}$ values. Each reaction was performed in duplicate, and at least three independent determinations of each IC$_{50}$ were made. To determine K_m values for ATP, initial velocities of kinase reaction were determined for eight different ATP concentrations ranging from 15 to 0 mM using 3-fold dilution steps and four time points. These velocities were fitted to the Michaelis−Menten equation ($V = V_{\text{max}}*S/(K_m + S)$) using the XLfit add-on for Microsoft Excel to yield the values for K_m and V_{max}, the maximal velocity for the reaction catalyzed by the given amount of kinase.

2.6. Compound Synthesis. Details on the synthesis and characterization of a focused library of type III pyrazolourea and type II quinoline− and quinazoline−pyrazolourea hybrid inhibitors are provided in the Supporting Information.

2.7. Protein Crystallography. Various inhibitors were cocrystallized with wild-type p38α using conditions similar to those previously reported for unmodified p38α.[20] Briefly, protein−inhibitor complexes were prepared by mixing 30 μL of p38α (10 mg/mL) with 0.3 μL of inhibitor (100 mM in DMSO) and incubating the mixture for 1−2 h on ice. Samples were centrifuged at 13 000 rpm for 5 min to remove excess inhibitor. Crystals were grown in 24-well crystallization plates using the hanging drop vapor diffusion method and by mixing 1.5 μL of protein−inhibitor solution with 0.5 μL of reservoir (100 mM MES pH 5.6−6.2, 20−30% PEG4000, and 50 mM n-octyl-β-D-glucopyranoside).

2.8. Data Deposition. All crystal structures described were deposited into the Protein Data Bank (PDB codes: 3GCP, 3GCQ, 3GCS, 3GCU, 3GCV).

3. Results

3.1. Selection of the Labeling Position on the Activation Loop. High-resolution crystal structures of human p38α in complex with type I, type II, or type III inhibitors have provided a wealth of structural detail about both the active and the inactive conformation, led to the deposition of 90 complex structures into the protein data bank (PDB), and have spurred the design of diverse inhibitor classes. This wealth of structural knowledge also made p38α an ideal candidate for the development of a fluorescence-based direct binding assay that allows for the detection and characterization of inhibitors, which bind to the DFG-out conformation. The principle of the fluorescent-labeled p38α assay for allosteric binders is highlighted in Figure 1a. The fluorophores we employed for labeling are commonly used to generate fluorescent protein conjugates, are relatively small in size, and are sensitive to polarity and/or conformational changes. Acrylodan is known to produce a typically robust response[18,21] and was expected to be especially sensitive to movements of the activation loop upon binding of DFG-out binders.

Prior to labeling the kinase, we first analyzed several crystal structures of p38α in the DFG-in and DFG-out conformations to identify the most suitable fluorophore attachment site in the activation loop. Care was taken to choose an amino acid position that exhibits significant movement upon ligand binding and is solvent-exposed to enable the attachment of a fluorophore added in solution. Sequence alignments of the activation loop of several human kinases (Figure 1b) were also used to avoid mutating common phosphorylation sites (and adjacent or nearby residues) or highly conserved regions or positions known to be involved

(19) Hibbs, R. E.; Talley, T. T.; Taylor, P. *J. Biol. Chem.* **2004**, *279*, 28483−91.

(20) Bukhtiyarova, M.; Northrop, K.; Chai, X.; Casper, D.; Karpusas, M.; Springman, E. *Protein Expression Purif.* **2004**, *37*, 154−61.

(21) Richieri, G. V.; Ogata, R. T.; Kleinfeld, A. M. *Mol. Cell. Biochem.* **1999**, *192*, 87−94.

(22) Thompson, J. D.; Gibson, T. J.; Higgins, D. G. *Curr. Protoc. Bioinformatics* **2002**, 23.
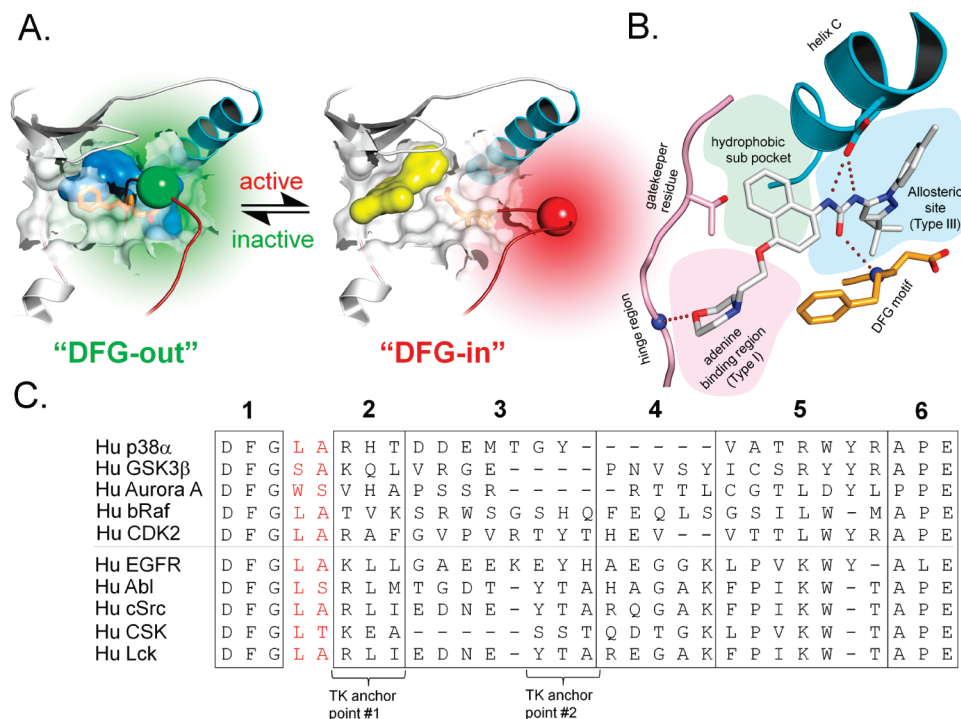
Figure 1. Schematic diagram of the fluorescent kinase binding assay. (a) Kinases such as p38α exist in both inactive (left) and active (right) states depending on the orientation of the DFG motif (orange sticks) and the activation loop (red). The binding of type II/III (represented by blue surface) and type I ligands (represented by yellow surface) can stabilize either the inactive DFG-out or the active DFG-in conformations, respectively, and induce conformational changes, which can be detected by different fluorophores (differently colored spheres). (b) Schematic representation of the binding mode of the type II inhibitor BIRB-796 in p38α (PDB code: 1kv2) highlights the different regions of the binding site utilized by different inhibitor types. (c) Sequence alignment of several kinase activation loops guides labeling of the DFG+1 and DFG+2 positions as the most suitable for labeling the kinase (red text). Regions that are highly conserved or crucial to kinase structural stability or enzymatic activity are shown (boxed regions). Alignments were performed using Clustal W.[22]

in key structural interactions that are crucial to kinase regulation. The activation loop sequence is bookended by the highly conserved DFG (box 1) and APE motifs (box 6). The DFG+3 position is commonly a basic amino acid, which interacts directly with the primary phosphorylation site of the activation loop.[23] The DFG+3 through DFG+5 (box 2) serves as a hydrophobic anchor point with other structural features of the C-lobe in tyrosine kinases.[24] This is followed by a variable length segment (box 3−4) contains a high incidence of Tyr, Ser, and Thr residues, which can be phosphorylated. The C-terminal end of the activation loop (box 5) forms several interactions with the C-lobe of the kinase and is important in substrate binding.

We found that residues immediately following the DFG motif (DFG+1 and DFG+2) at the N-terminal end of the activation loop exhibit significant movement with conformational changes and are typically not associated with disease-related genetic alterations known to influence kinase activity.[25] Additionally, sequence alignments of all human kinases reveal that at least 47 kinases have a naturally occurring Cys in these two positions, suggesting that mutation of the labeling site residue to Cys would likely be tolerated. Therefore, Ala172 of p38α (DFG+2 position) was subsequently mutated into a Cys for specific reaction with thiol-reactive fluorophores. We also used available structural information to identify solvent-exposed Cys, which

could undesirably react with the fluorophore. We determined that only two of the four Cys in p38α were solvent-exposed (Cys119 and Cys162) and subsequently mutated these into Ser to increase the probability that the kinase would be singly labeled only on the activation loop, which was ultimately confirmed by mass spectrometry methods (Figure S1). In the case where no structures are available for a kinase of interest, a variety of online modeling tools can be used to generate DFG-in and DFG-out conformational models for the same amino acid sequence (Supporting Information). Additionally, the use of published screening data of various inhibitor types against a panel of kinases[26] may be a useful tool for assessing whether or not the kinase of interest is capable of adopting the DFG-out conformation, which is necessary for the assay to succeed.

3.2. Fluorescence Characterization of Fluorescent−p38α Conjugates. The newly introduced Cys at position 172 of p38α was labeled with various thiol-reactive fluorophores reported to be sensitive to the polarity of their surrounding microenvironment. The fluorescent properties of each labeled kinase were characterized by inducing the DFG-out conformation using the well-known p38α type II inhibitor, BIRB-796. Using the fluorescence spectra obtained for labeled p38α in the presence and absence of a saturating concentration of BIRB-796, we calculated ΔI_{std}, the normalized intensity change as compared to average intensity, and ΔR_{max}, the maximal standard intensity change at two wavelengths (Supporting Information). These parameters are two of the most important criteria for identifying ideal fluorophore−protein conjugates for fluorescence studies.

(23) Nolen, B.; Taylor, S.; Ghosh, G. *Mol. Cell* **2004**, *15*, 661–75.
(24) Levinson, N. M.; Seeliger, M. A.; Cole, P. A.; Kuriyan, J. *Cell* **2008**, *134*, 124–34.
(25) Torkamani, A.; Kannan, N.; Taylor, S. S.; Schork, N. J. *Proc. Natl. Acad. Sci. U.S.A.* **2008**, *105*, 9011–6.

(26) Karaman, M. W. *Nat. Biotechnol.* **2008**, *26*, 127–32.

Fluorophore	λ_{exc} (nm)	$\lambda_{max, apo}$ (nm)	$\lambda_{max, sat}$ (nm)	ΔI_{std}	ΔR_{max}	k_{obs} (100 nM BIRB-796)		K_{eq}
						Assoc. (x10⁻⁴ s⁻¹)	Dissoc. (x10⁻⁵ s⁻¹)	
Acrylodan	386	468	514	**0.50**	**1.26**	6.9 ± 2.2	5.1 ± 0.8	0.074
IAEDANS	360	463	469	**0.80**	0.33	30.3 ± 10.1	22.1 ± 1.6	0.073
Fluorescein	495	519	520	**1.00**	0.36	6.4 ± 1.8	16.7 ± 11.9	0.259
Pyrene	339	384	384	**0.83**	0.56	17.7 ± 4.9	37.1 ± 2.1	0.209
NBD	455	535	535	**0.73**	0.20	12.7 ± 4.7	18.4 ± 1.9	0.145
Atto680	680	689	699	**1.42**	0.34	6.7 ± 2.7	8.3 ± 0.6	0.125

Figure 2. Thiol-reactive fluorophores tested in the fluorescent kinase assay. Several fluorophores were conjugated to A172C of p38α, and their changing fluorescence properties were examined upon binding of BIRB-796, a known DFG-out binder of p38α. All values for ΔR_{max} and ΔI_{std} that meet the criteria deemed ideal fluorophore−protein conjugates[18] appear in bold. The superior ΔR_{max} of acrylodan is the result of a ∼45 nm shift in emission maxima in the DFG-out conformation. IAEDANS, a structural analogue of acrylodan, does not exhibit a large emission shift, but there is an increase in emission at ∼515 nm relative to ∼470 nm, allowing reliable binding curves to be measured despite the suboptimal ΔR_{max}. Pyrene and fluorescein are considerably more bulky than the other fluorophores and appear to enhance BIRB-796 dissociation rates, resulting in higher calculated equilibrium constants (K_{eq}) for 100 nM BIRB-796 under these experimental conditions. [Note: The chemical structure of Atto680 has not been released by the manufacturer (http://www.innovabiosciences.com).]

Ideally, values for ΔI_{std} should be >0.25 and values for ΔR_{max} should be >1.25.[18] According to these criteria, acrylodan-labeled p38α (ac-p38α) is the most ideal probe for a fluorescence-based assay for detecting DFG-out binders (Figure 2).

Ac-p38α allows for ratiometric measurements because DFG-out binders induce a shift in the emission maximum from 468 to 514 nm, indicative of the movement of acrylodan from a less polar to a more polar environment.[19,27] This feature is advantageous because ratiometric fluorescence measurements correct for dilution and pipetting errors between different samples in a titration series and produce reliable end point measurements. Although all other fluorophores examined showed a change in fluorescence upon ligand binding, they did not produce reliable binding curves (IAEDANS was an exception). However, all fluorescent kinase conjugates were acceptable with respect to ΔI_{std} and were suitable for making sensitive kinetic measurements of ligand binding and dissociation (Supporting Information and Figures S2 and S3).

In a final step, we characterized the kinetic properties of the wild type, mutated/unlabeled, and mutated/acrylodan-labeled p38α to determine the effects of the mutations and labeling on the activity of the kinase. In general, we found a 25-fold reduction in ATP K_m in the mutated kinase with no additional reduction in the ATP K_m with the attachment of an acrylodan, suggesting that the mutations do disrupt the affinity of p38α. Although it is not surprising that alterations to the activation loop would have some effect on kinase activity, these manipulations did not result in a kinetically dead kinase as we demonstrated previously for cSrc kinase.[28] IC50 values were then determined for type I and type II inhibitors in an activity-based assay, and only minor differences between the different kinase

constructs were observed for each inhibitor (Table S1). Thus, although the ATP K_m was increased significantly in the mutated kinase constructs used for labeling, these changes did not correlate with significant changes to inhibitor activity or affinity.

3.3. End Point and Real-Time Measurements: Determination of K_d, k_{on}, and k_{off}. End point measurements of ac-p38α using a dual-wavelength ratio (R = 514 nm/468 nm) allowed for direct and reliable K_d determination of type III and type II DFG-out binders. At each inhibitor concentration, the emission spectrum was measured (Figure 3a), and R was either plotted to show the saturation of ac-p38α in the inactive state (Figure 3b) or plotted on a logarithmic scale to directly determine the K_d (Figure 3c). Similar types of measurements were also possible with IAEDANS-p38α (Figure S2).

A significant change of emission at 468 nm also allowed for the possibility of studying the kinetics of dissociation (k_{off}) and association (k_{obs}) in real-time for different concentrations of ligand. Following addition of inhibitor, the fluorescence emission at 468 nm decreased in a dose-dependent manner and was nicely fit to a first-order kinetic (Figure 3d). These types of experiments yielded rate constants (k_{obs}) that were then plotted and fit linearly to obtain the k_{on} for the ligand (Figure 3e), which we found to be $(4.3 \pm 0.8) \times 10^3$ M⁻¹ s⁻¹ ($n = 3$) for BIRB-796. Alternatively, addition of a 10-fold molar excess of unlabeled p38α to ac-p38α prebound with ligand resulted in extraction of BIRB-796, a first-order increase in fluorescence, and direct determination of k_{off} (Figure 3f), which we found to be $(5.1 \pm 0.5) \times 10^{-5}$ s⁻¹ ($n = 3$). Both kinetic values differ by a factor of 10 from those published elsewhere for BIRB-796 using alternative methods.[8] Determination of k_{on} and k_{off} also allows for the indirect/calculated determination of K_d values ($K_d = k_{off}/k_{on}$) and sheds light on the factors contributing to different ligand affinities. Such rate measurements were possible with all fluorescent−p38α conjugates tested in this study (Figure S3). Last, these measurements demonstrate the reversibility of the fluorescence response and demonstrate the changing equilibrium that exists between the DFG-in and DFG-out conformations.

In experiments analogous to those shown in Figure 3d−f for BIRB-796, we used ac-p38α to determine the k_{on} and k_{off} for the smaller type III pyrazolourea analogue **1** (structure shown in Figure 4) to be $(6.6 \pm 1.2) \times 10^3$ M⁻¹ s⁻¹ ($n = 3$) and $(7.1 \pm 3.2) \times 10^{-3}$ s⁻¹ ($n = 3$), respectively. Both values are different from previously published values by 2 orders of magnitude.[8] The differences in measured kinetic values for BIRB-796 and **1** are likely a consequence of the different assay systems employed in each study. In the studies reported by Pargellis et al., the dissociation of these compounds from p38α was measured by the binding of an ATP-competitive inhibitor of p38α, SKF86002, which becomes highly fluorescent upon binding. The binding of SKF86002 shifts the kinase more toward the DFG-in conformation, resulting in the dissociation of pyrazolourea compounds from the adjacent allosteric site as the DFG Phe flips back toward the allosteric pocket. Conversely, the displacement of prebound SKF86002 was used to measure the binding of pyrazoloureas. However, it is possible that the displacement of low nanomolar affinity ligands such as BIRB-796 ($K_d = 0.1$ nM[8]) by the weaker inhibitor SKF86002 ($K_d = 180$ nM[8]) is not an optimal approach and may result in slower apparent k_{off} values and lower apparent K_d values. Thus, K_d values determined in this manner may be more subject to the experimental conditions under which the rate constants are determined.

(27) Richieri, G. V.; Ogata, R. T.; Kleinfeld, A. M. *J. Biol. Chem.* **1992**, *267*, 23495−501.
(28) Simard, J. R.; Kluter, S.; Grutter, C.; Getlik, M.; Rabiller, M.; Rode, H. B.; Rauh, D. *Nat Chem Biol.* **2009**, *5*, 394−6.
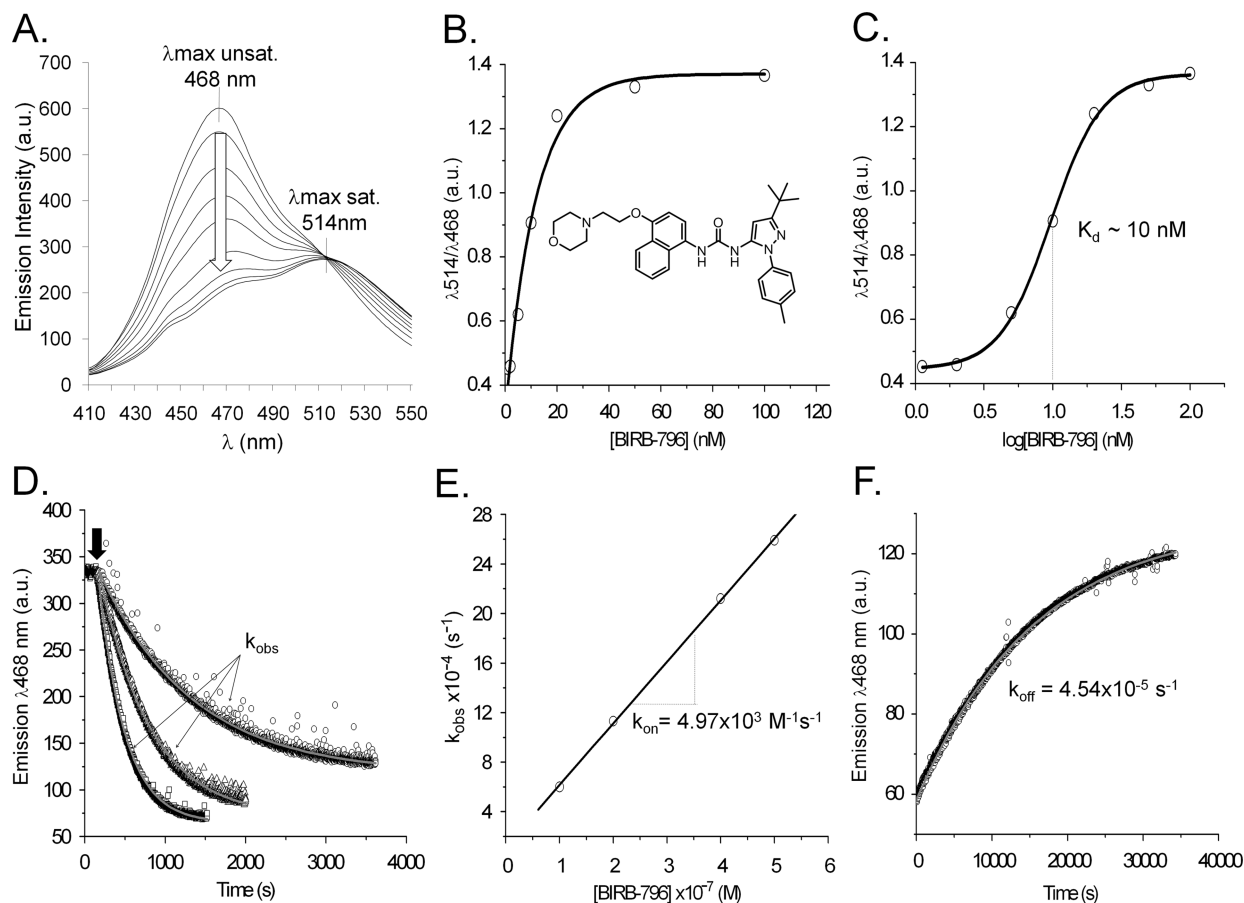
Figure 3. Real-time and end point fluorescence measurements using ac-p38α labeled on the activation loop. (a) Acrylodan emission at 468 nm decreases upon binding of BIRB-796, a known DFG-out binder of p38α, resulting in a red-shift of the maximum emission wavelength in the bound state. End point equilibrium measurements can be made to directly obtain the K_d. (b) Ratiometric fluorescence data (R = 514 nm/468 nm) were plotted to show the saturation of the inactive state or (c) on a logarithmic scale of inhibitor concentration to obtain the K_d. Fluorescence traces can also be measured in real-time at a single wavelength (468 nm) to determine various kinetic rate constants. (d) The fluorescence decay resulting from the addition of different amounts of BIRB-796 (large arrow) was fit to a first-order decay function to obtain k_{obs}. (e) Experimentally determined k_{obs} values can be plotted to determine k_{on} for BIRB-796. (f) Extraction of BIRB-796 from ac-p38α using an excess of unlabeled p38α allowed direct determination of k_{off}, which was also fit to a first-order function. The data presented above are representative of a typical set of experiments carried out for BIRB-796 and other DFG-out binders using ac-p38α.

The optimal method for accurately measuring the affinity of any ligand to a protein is to directly measure the formation of the ligand−protein complex as demonstrated with our approach. However, we were still able to observe that the K_d values of different pyrazoloureas were more influenced by k_{off} rather than k_{on}, an effect that is well-documented in the case of p38α.[8] Furthermore, we were able to validate the conditions used to measure our kinetic rate constants by using them to calculate K_d values of 11.9 ± 1.3 nM and 1.079 ± 0.347 μM for BIRB-796 and **1**, respectively. These values compare well with the direct K_d values determined directly using end point measurements in which values of 7.5 ± 1.9 nM (n = 3) and 1.19 ± 0.14 μM (n = 3) for BIRB-796 and **1** were measured, respectively.

3.4. SAR of a Focused Pyrazolourea Compound Library. We designed and generated a focused library of pyrazoloureas, a class of compounds whose pharmacophore and binding mode are known in p38α, and used several new derivatives of this scaffold to examine structure−activity relationships (SAR) and characterize the fluorescence response of ac-p38α. Pyrazoloureas represent one of the prototypes for type III and type II kinase inhibitors. Type III pyrazoloureas not only stimulated the development of the former clinical candidate BIRB-796[10] but also provided a wealth of structural, binding, and dissociation

data, allowing for comparison of K_d values determined here using ac-p38α (Figure 4) with other approaches.[8,11,29] Several of these known compounds were also synthesized to serve as a measuring stick for our fluorescent-tagged kinase binding assay.

As expected, the K_d of **6** (BIRB-796) was time-dependent (Figure S4) as reported elsewhere.[8] All type III inhibitors also showed this time dependence, but required less time (2−4 h) to reach equilibrium with p38α. Thus, long preincubation times are necessary to ensure complete binding of type II and type III ligands before making end point measurements. In general, we found excellent agreement between our K_d values and those reported elsewhere for known compounds using other approaches, with the largest differences occurring for compounds with a published K_d of <10 nM. As discussed above for BIRB-796, the affinity of DFG-out binders to p38α is dictated primarily by k_{off}. Therefore, we believe that the calculated K_d values reported in the literature for the strongest binders are more subject to the experimental conditions under which k_{off} was measured and have been shown to vary significantly depending on the methods used.[29] However, certain trends in

(29) Kroe, R. R.; Regan, J.; Proto, A.; Peet, G. W.; Roy, T.; Landro, L. D.; Fuschetto, N. G.; Pargellis, C. A.; Ingraham, R. H. *J. Med. Chem.* **2003**, *46*, 4669–75.
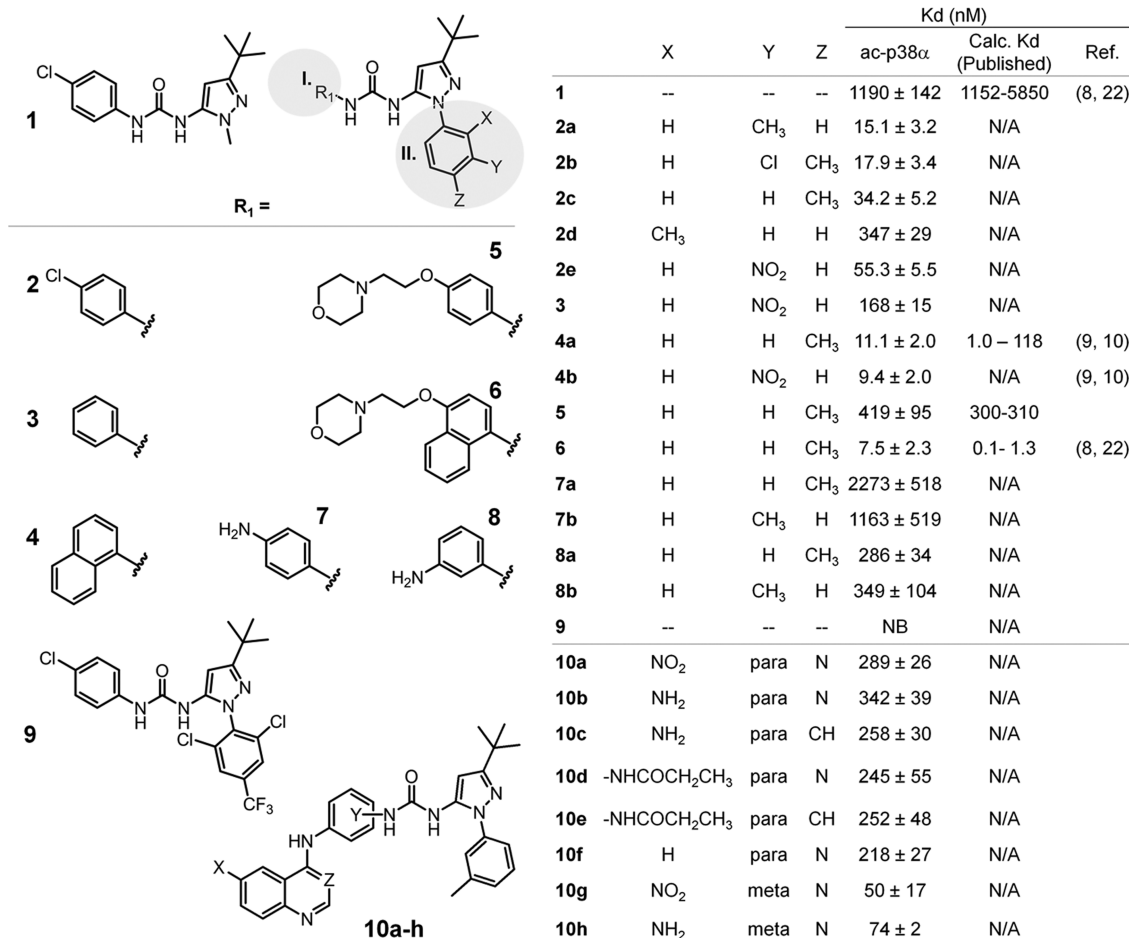
	X	Y	Z	Kd (nM) ac-p38α	Calc. Kd (Published)	Ref.
1	--	--	--	1190 ± 142	1152-5850	(8, 22)
2a	H	CH₃	H	15.1 ± 3.2	N/A	
2b	H	Cl	CH₃	17.9 ± 3.4	N/A	
2c	H	H	CH₃	34.2 ± 5.2	N/A	
2d	CH₃	H	H	347 ± 29	N/A	
2e	H	NO₂	H	55.3 ± 5.5	N/A	
3	H	NO₂	H	168 ± 15	N/A	
4a	H	H	CH₃	11.1 ± 2.0	1.0 – 118	(9, 10)
4b	H	NO₂	H	9.4 ± 2.0	N/A	(9, 10)
5	H	H	CH₃	419 ± 95	300-310	
6	H	H	CH₃	7.5 ± 2.3	0.1- 1.3	(8, 22)
7a	H	H	CH₃	2273 ± 518	N/A	
7b	H	CH₃	H	1163 ± 519	N/A	
8a	H	H	CH₃	286 ± 34	N/A	
8b	H	CH₃	H	349 ± 104	N/A	
9	--	--	--	NB	N/A	
10a	NO₂	para	N	289 ± 26	N/A	
10b	NH₂	para	N	342 ± 39	N/A	
10c	NH₂	para	CH	258 ± 30	N/A	
10d	-NHCOCH₂CH₃	para	N	245 ± 55	N/A	
10e	-NHCOCH₂CH₃	para	CH	252 ± 48	N/A	
10f	H	para	N	218 ± 27	N/A	
10g	NO₂	meta	N	50 ± 17	N/A	
10h	NH₂	meta	N	74 ± 2	N/A	

Figure 4. Measured K_d values and SAR of a focused library of pyrazoloureas. The synthesis and characterization of all pyrazolourea derivatives are described in the Supporting Information. All compounds were titrated against ac-p38α (50 nM) over a concentration range of 1 nM to 20 μM to generate binding curves using the ratiometric fluorescence change ($R = 514$ nm/468 nm) observed upon binding to the DFG-out conformation of p38α. K_d values for each compound were then directly obtained from the binding curves. All reported values represent the mean ± s.d. from at least three independent titrations.

the SAR are always maintained with respect to aryl moiety I (substituted phenyl attached to the urea) and aryl moiety II (substituted phenyl attached to the pyrazole) regardless of the assay system used to make the measurements.

In the case of aryl moiety I, we observed a noticeable affinity ranking such that **3** (phenyl) < **2e** (4-chlorophenyl) < **4b** (naphthyl), a SAR trend that is well-documented.[8,10,11,29,30] Moiety I fits into a small hydrophobic subpocket behind the gatekeeper residue of p38α, and the bulkier naphthyl moiety forms better lipophilic interactions as a result of its ability to penetrate deeper into this subpocket. It could also be argued that more solvation entropy is gained (release of more water molecules) upon burial of the bulkier naphthyl in this subpocket.[31] Thus, a phenyl moiety alone at this position does not contribute significantly to the affinity of the compound, explaining the much higher K_d of **3** in comparison to **2e** and **4b**. This is further confirmed by **5**, which has a central phenyl in place of the bulkier naphthyl of **6** (BIRB-796), resulting in a 50-fold higher K_d. Similar findings for these compounds were also observed elsewhere using other

approaches.[10] Given the hydrophobic characteristics of this subpocket, it is also not surprising to see a significant loss of affinity for the more polar 4-aminophenyl **7** or 3-aminophenyl **8** type III derivatives.

The addition of a monosubstituted aryl moiety II to the N1 of the pyrazole of **1** extends the ligand into the allosteric pocket and results in a significant increase in the affinity. This phenyl ring shows a distinct preference for substituents in the para and meta positions in our assay, a SAR trend that is also well-documented.[10] To further investigate the importance of the substitution pattern of moiety II, we used the crystal structure of p38α in complex with BIRB-796 (PDB-code: 1kv2) together with in silico modeling to design and synthesize a bulkier inhibitor **9** (**RL19**). We hypothesized that the combination of a 4-trifluoromethyl and 2,6-dichloro substitution pattern on the phenyl ring would prevent the compound from fitting into the allosteric pocket, which was confirmed by the complete lack of fluorescence response from ac-p38α.

Recently, we reported the development of several type II quinazoline−pyrazolourea hybrid inhibitors of cSrc kinase.[15] In the case of cSrc, smaller type III pyrazoloureas were found to inhibit cSrc with mid micromolar IC₅₀ values. In a manner similar to the development of BIRB-796 from **1**,[10] the fusion of these compounds with a quinazoline scaffold, which are also

(30) Regan, J.; Capolino, A.; Cirillo, P. F.; Gilmore, T.; Graham, A. G.; Hickey, E.; Kroe, R. R.; Madwed, J.; Moriak, M.; Nelson, R.; Pargellis, C. A.; Swinamer, A.; Torcellini, C.; Tsang, M.; Moss, N. *J. Med. Chem.* **2003**, *46*, 4676–86.
(31) Lafont, V.; Armstrong, A. A.; Ohtaka, H.; Kiso, Y.; Mario Amzel, L.; Freire, E. *Chem. Biol. Drug. Des.* **2007**, *69*, 413–22.

micromolar inhibitors of cSrc,[32] resulted in potent low nanomolar type II inhibitors that extend into the ATP binding site to interact with the hinge region. Furthermore, we showed that the 1,4-*para* fused hybrids **10a**, **10b**, and **10d** were better binders to cSrc while using molecular modeling to predict that p38α would better accommodate the 1,3-*meta* fused inhibitors **10g** and **10h**. Using ac-p38α, we were able to confirm this hypothesis and found that **10g** and **10h** have a 6-fold higher affinity over **10a** and **10b**. We solved the crystal structure of **10h** (**RL62**) and **10b** (**RL45**) each in complex with p38α and observed additional stabilizing interactions, which explain why 1,3-*meta* hybrids have a higher affinity for p38α (Figure S5). We also performed an extensive analysis of the kinetic rate constants for these compounds using ac-p38α (Table S2) and found that the dissociation rate of **10h** is slower than that of **10b**, while both compounds exhibit similar k_{obs} for binding ($(1.40 \pm 0.25) \times 10^{-3}$ s^{-1} ($n = 3$) for **10h** and $(1.36 \pm 0.13) \times 10^{-3}$ s^{-1} ($n = 3$) for **10b**, respectively), which may partially account for the higher affinity of **10h**. Last, these detailed kinetic and structural characterizations of 1,3- and 1,4-fused hybrid compounds led us to design and synthesize several pyrazolourea−quinoline analogues as compounds that are potent type II inhibitors of p38α. Further details regarding the kinetic and structural characterization of these and additional hybrid compounds can be found in the Supporting Information.

3.5. Binding of Alternative Drug Scaffolds. Following our SAR studies of several pyrazolourea compounds, we investigated a number of commercially available type I and type II kinase inhibitors to confirm that our new assay system was not dependent on the pyrazolourea scaffold. Marketed drugs such as lapatinib (Tykerb) and imatinib (Gleevec), selective potent type II inhibitors of HER2 and Abl kinases, respectively, and the promiscuous type I inhibitor staurosporine did not trigger a significant fluorescence change (Figure S6A). Further screening revealed that the addition of sorafenib (Nexavar), a well-known b-Raf and VEGFR2 inhibitor, produced a strong fluorescence response and binds to ac-p38α with a K_d of 56 ± 5 nM ($n = 3$), which is within range of the published K_d against its intended kinase targets.[33] The K_d of sorafenib was also found to be time-dependent similar to other type II inhibitors. In a recent publication where 38 known kinase inhibitors were screened against a panel of 317 kinases,[26] the authors found that lapatinib, imatinib, and staurosporine do not bind appreciably to p38α ($K_d > 10$ μM), in strong agreement with our data. Interestingly, they found that sorafenib binds to p38α with a $K_d \approx 370$ nM, nearly 6-fold higher than our determined K_d value. Because we observed a time dependence for sorafenib binding to p38α over a period of 4 h, their higher K_d value may be due to the shorter 1 h preincubation used in that large screen.

To confirm that our new approach was correctly reporting the binding of sorafenib to the DFG-out conformation, we cocrystallized it with wild type p38α and solved the structure to a resolution of 2.1 Å (Figure S6B). Although the kinase is found in the DFG-out conformation and the inhibitor resides in the typical type II orientation, bridging the allosteric site and the hinge region of the kinase, the interaction of the ligand with the gatekeeper Thr and the hinge region of p38α differs from the previously reported sorafenib b-Raf complex (pdb code:

1uwh[34]) (Figure S6C). Further structural details are described in the Supporting Information.

3.6. Detection of ATP-Competitive Inhibitors/Identifying False Hits in Screens. In addition to several DFG-out binders, we also tested whether several known ATP-competitive inhibitors of p38α could be detected by ac-p38α and, if detected, to determine whether these compounds could be discriminated from DFG-out binders. The majority of compounds tested were not detected up to concentrations of 10 μM. However, a few imidazole derivatives, SKF86002 and SB203580, were detected with varying degrees of sensitivity. Through the use of fluorescence spectroscopy and protein X-ray crystallography, we were able to explain the detection of such compounds and found that real-time kinetic measurements of binding made with ac-p38α can be used to easily discriminate type I inhibitors should they be detected (Figure 5).

Using our ac-p38α assay, the type I inhibitor SKF86002 gave a binding curve with a K_d of 721 ± 36 nM (Figure 5A), which is significantly higher than the published value ($K_d \approx 180$ nM[8]), suggesting that ac-p38α is relatively insensitive to type I binders. We designed a simple experiment to confirm that ac-p38α loses the ability to accurately sense binding of type I ATP-competitive compounds. We used the intrinsic fluorescence of the inhibitor described above, SKF86002, to measure its binding to ac-p38α. It is known that this compound exhibits a very large increase in fluorescence emission upon binding to p38α.[8] Because the emission maxima of SKF86002 ($\sim$420 nm) and acrylodan ($\sim$470 nm) do not overlap, we added this compound to ac-p38α and made end point measurements to obtain a binding curve with a K_d of 78 ± 9 nM, which is 10-fold lower under the same experimental conditions than when measuring the fluorescence of acrylodan. Therefore, it is clear that the acrylodan label itself is insensitive to most type I binders, most likely due to the fact that the fluorescent-tagged activation loop is not expected to change conformations upon binding of these types of ligands. However, the binding of some type I inhibitors such as SKF86002 induce unexpected conformational changes involving the activation loop and/or a reorientation of the N-lobe relative to the C-lobe upon binding to the kinase hinge region. In the latter case, these localized conformational changes could modulate the polar environment in the vicinity of the fluorophore without movement of the activation loop, resulting in false hits when screening for DFG-out binders.

In another example, we identified SB203580 as a potent low nanomolar type I p38α inhibitor and close structural analogue of SKF86002. Surprisingly, the fluorescence change observed in ac-p38α upon binding of SB203580 was robust and allowed binding curves to be generated (Figure 5B), which gave K_d values that were the same as those previously published using other methods (15 ± 2 nM).[10] To better understand why this compound in particular triggered such a sensitive response, we cocrystallized it with p38α (Figure 5C). The structure was solved to a resolution of 2.3 Å with positive difference density for the inhibitor clearly visible in the ATP binding pocket. Although the pyridinyl group of the inhibitor forms a hydrogen bond to the hinge region, which qualifies SB203580 as a type I inhibitor, the kinase adopted the DFG-out conformation. The plane of the methylsulfinyl substituted phenyl is sandwiched between the DFG motif and the P-loop and forms $\pi-\pi$ stacking interactions with the side chains of Tyr35 (glycine-

(32) Michalczyk, A.; Kluter, S.; Rode, H. B.; Simard, J. R.; Grutter, C.; Rabiller, M.; Rauh, D. *Bioorg. Med. Chem.* **2008**, *16*, 3482–8.

(33) Wilhelm, S.; Carter, C.; Lynch, M.; Lowinger, T.; Dumas, J.; Smith, R. A.; Schwartz, B.; Simantov, R.; Kelley, S. *Nat. Rev. Drug Discovery* **2006**, *5*, 835–44.

(34) Wan, P. T.; Garnett, M. J.; Roe, S. M.; Lee, S.; Niculescu-Duvaz, D.; Good, V. M.; Jones, C. M.; Marshall, C. J.; Springer, C. J.; Barford, D.; Marais, R. *Cell* **2004**, *116*, 855–67.
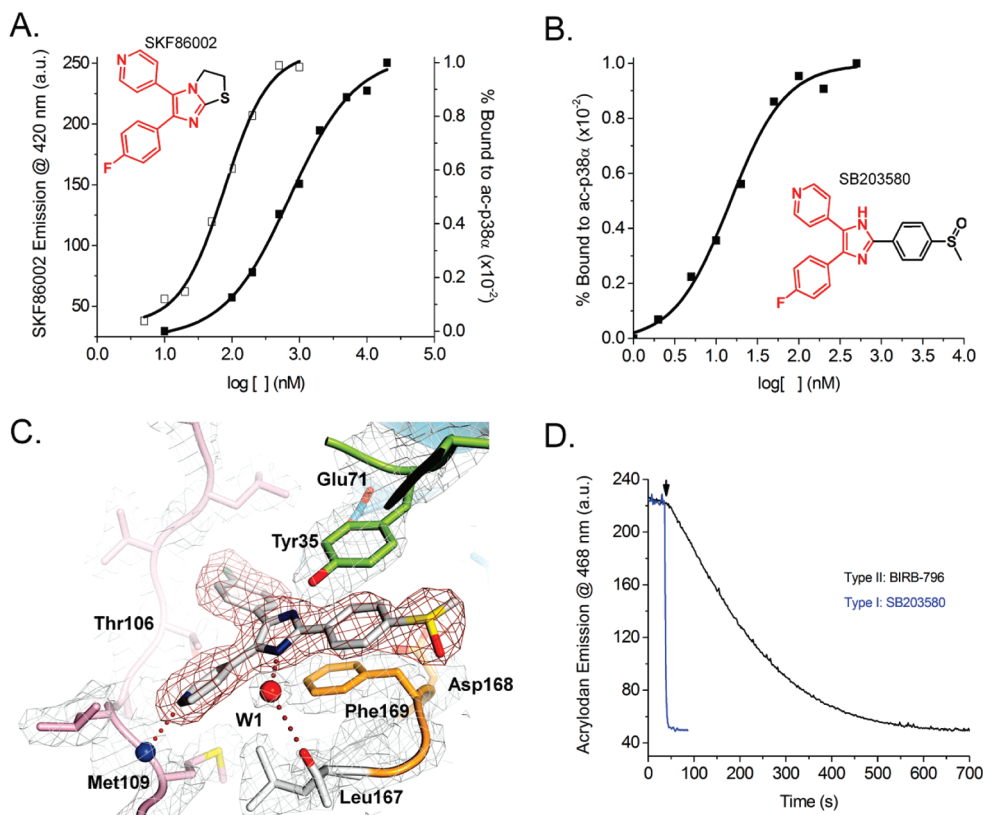
Figure 5. Detection of the binding of imidazole derivatives SB203580 and SKF86002 by ac-p38α. The high affinity ATP-competitive inhibitor of p38α, SKF86002, binds with a $K_d \approx 78$ nM (□) according to changes in the fluorescence emission of the inhibitor itself upon binding (left axis), while the ratiometric fluorescence of acrylodan (right axis) reports a K_d of 721 nM (■) (A). SB203580 shares structural moieties (red) similar to SKF86002 and produced a binding curve with a K_d of 15 nM when added to ac-p38α (B). We solved the crystal structure of SB203580 to 2.3 Å, and electron density maps of SB203580 (red) and p38α (gray) are contoured to 1σ. Possible hydrogen-bonding interactions are highlighted by dotted lines. The pyridine ring of the inhibitor forms an essential hydrogen bond to the hinge region (Met109) of the kinase. The proximal phenyl substituent is perfectly sandwiched between the side chain of Phe169 of the DFG-motif (orange) and the side chain of Tyr35 of the glycine-rich loop (green) respectively. The methylsulfinyl substituted phenyl is electron rich and forms energetically favorable $\pi-\pi$ interactions with the side chains of Tyr35 and Phe169 and most likely stabilizes the DFG-motif in the "out" conformation. In addition, water molecule W1 bridges a hydrogen bond between N3 of the imidazole of the inhibitor and the backbone carbonyl (red) of Leu167 and is likely to contribute to stabilization of the DFG-out conformation (C). For real-time kinetic measurements, a single dose of BIRB-796 or SB203580 (10 μM) was added to ac-p38α (0.1 μM). ATP-competitive inhibitors always produce an instantaneous change in fluorescence (blue trace), while slower binding DFG-out stabilizing inhibitors (black trace) typically take several minutes to reach equilibrium (D).

rich loop) and Phe169 (DFG motif). The N3 of the imidazole moiety hydrogen bonds via a water molecule to the backbone of Leu167 located at the N-terminal end of the DFG motif. The net result of these interactions is the stabilization of p38α in the DFG-out conformation despite the type I binding mode of SB203580. Although the compound is not bound within the allosteric site, the assay detected the compound due to this unique binding mode.

Interestingly, SB203580 has been analyzed extensively by both protein X-ray crystallography and NMR techniques (PDB codes: 2ewa[17] and 1a9u[35]). While one study reported the binding of SB203580 to the DFG-in conformation,[35] the other group reported that this inhibitor can in fact bind to both DFG-conformations (~50% inhibitor occupancy in each conformation) and further confirmed this finding using 2D-NMR experiments.

We can postulate on the basis of these observations that SKF86002 may bind in a similar manner to SB203580. Both compounds share structural similarities, in particular the 4-fluorophenyl moiety, which likely extends back into the hydrophobic

subpocket behind the gatekeeper as observed for SB203580. The core Y-shaped structure of these compounds is exactly the same, with the exception of the additional phenyl moiety of SB203580, which is responsible for forming the $\pi-\pi$ stacking interactions with Phe169 and Tyr35 of p38α to stabilize the DFG-out conformation. This ring is not present in SKF86002. Assuming the binding mode is similar, this structural difference may reduce the ability of SKF86002 to stabilize the DFG-out conformation, thus explaining the observed insensitivity of the acrylodan-labeled activation loop to its binding, in contrast to its highly sensitive response to SB203580. Regardless of this insensitivity to most type I inhibitors, the assay appears to be very sensitive to type I binders that interact and modulate the conformation of the DFG motif and, thus, the activation loop.

It is known that the kinase activation loop and helix C, which forms the "roof" of the allosteric pocket, are both in cross-talk with the glycine-rich loop,[34,36–38] a structural element that serves as a regulatory flap above the ATP binding site. This loop can interact directly with some type I inhibitors, often contributing

(35) Wang, Z.; Canagarajah, B. J.; Boehm, J. C.; Kassisa, S.; Cobb, M. H.; Young, P. R.; Abdel-Meguid, S.; Adams, J. L.; Goldsmith, E. J. *Structure* **1998**, *6*, 1117–28.

(36) Hanks, S. K.; Hunter, T. *FASEB J.* **1995**, *9*, 576–96.
(37) Mapelli, M.; Massimiliano, L.; Crovace, C.; Seeliger, M. A.; Tsai, L. H.; Meijer, L.; Musacchio, A. *J. Med. Chem.* **2005**, *48*, 671–9.
(38) Wong, L. *J. Mol. Biol.* **2005**, *351*, 131–43.

to their increased affinity, as demonstrated for the potent Abl kinase inhibitor nilotinib.[39] Thus, we expect that the interaction of this structural element with some type I inhibitors will change the environment of the acrylodan without actually inducing a movement of the activation loop. Acrylodan responds to any change in the local environment, whether induced directly by the movement of the activation loop or indirectly by the movement of nearby elements such as helix C or the glycine-rich loop.

As a result of these findings, it is likely that some type I inhibitors may register as false hits in future large screening campaigns for DFG-out binders. Therefore, it was necessary to determine whether or not these ligands could be discriminated from DFG-out binders using our assay. Using the cuvette method, we were able to accomplish this by looking at the kinetics of the fluorescence changes in real time. In the case of DFG-out binders such as BIRB-796, the kinetic is relatively slow (Figure 5D, Figure 3E), and the fluorescence change takes several minutes to reach completion. However, in the case of ATP-competitive inhibitors such as SB203580, the induced fluorescence change is instantaneous (2−4 s). This is not surprising because the ATP binding site is relatively easy to access in comparison to the allosteric site, which only becomes available when the kinase samples the DFG-out conformation. This instantaneous fluorescence response was also observed for SKF86002 (data not shown).

4. Discussion

Although kinase inhibitor drug discovery has progressed dramatically in the past decade and resulted in almost a dozen marketed drugs,[3,4] several challenges such as inhibitor selectivity of classical ATP-competitive inhibitors and kinase drug resistance remain. A high number of known type I kinase inhibitors are more sensitive to drug resistance, and limited selectivity may be a direct consequence of their discovery using enzymatic assays to screen large compound libraries.[1] Because these assays rely on the kinase to be phosphorylated and in the active conformation, its ability to adopt the inactive conformation is reduced, resulting in an enrichment of hits of type I scaffolds. Because most of the chemical scaffolds that qualify as ATP-competitive ligands have already been discovered, classical kinase activity assays are becoming more obsolete for the discovery of more specific novel compounds to serve as lead structures for future medicinal chemistry and chemical biology research. This points toward current medicinal chemistry endeavors to identify and develop inhibitors that target alternative binding sites and stabilize inactive kinase conformations.[1,40−43] This is also of benefit to the pharmaceutical industry, which is beginning to struggle to identify new patentable drug scaffolds for kinases. However, the shifting focus has resulted in an

additional bottleneck, the current lack of suitable high-throughput methods that can discriminate between DFG-in and DFG-out binders. To date, no method exists for predicting whether a kinase of interest can even be inhibited in this manner.

To address these needs, we developed a novel assay system to monitor transitions in kinase conformation induced and stabilized by the binding of certain ligand types. Our assay substantially differs from kinase assays that are widely employed in pharmaceutical and chemical biology research, which exclusively monitor kinase activity in a classical sense via phosphorylation of various substrates. We utilized our new assay for detailed kinetic characterization of a diverse collection of known and unknown kinase inhibitors and found that the system is highly sensitive to type II/III inhibitors and insensitive to most ATP-competitive inhibitors in the case of p38α. However, we demonstrated that some unique type I binders such as SB203580, which unexpectedly induce and stabilize the DFG-out conformation, are sensitively detected as well but can easily be discriminated from type II or III binders by looking at the binding kinetics. Thus, the labeling of kinases that are regulated by a DFG-in/DFG-out conformational equilibrium with a suitable fluorophore will not only allow for the detection of the ligand-induced transition between kinase conformations, but also provides a unique handle to easily discriminate between different inhibitor types.

We recently used this approach to identify the first known type III ligands of cSrc kinase and successfully optimized these scaffolds into potent low nanomolar type II inhibitors, some of which remained potently active against common drug resistance mutations.[15,28] The findings provide proof that this direct binding assay extends well into emerging medicinal chemistry research. In the past, the detection of ligand binding was often evaluated by protein X-ray crystallography to unravel the binding mode of the ligand. This is a standard procedure in modern structure-based drug design. Along these lines, we demonstrated that the b-Raf/VEGFR inhibitor sorafenib is detected by our assay with remarkable affinity and adopts a type II binding mode in which a new kind of interaction is formed between the inhibitor, the gatekeeper and the hinge region of p38α, features which could prove valuable to direct further compound design.

5. Conclusions

The development of inhibitors that stabilize inactive (DFG-out) kinase conformations is moving to the forefront of kinase inhibitor research. To allow for the sensitive and reliable identification of DFG-out stabilizers from compound libraries, we developed a novel fluorescence-based binding assay using the serine−threonine kinase p38α as a model system. We utilized known kinase inhibitors as well as newly designed compounds to validate this system and confirmed our results with protein X-ray crystallography. In doing so, we were able to identify the b-raf inhibitor sorafenib as a high affinity binder of p38α and also observed a unique type II inhibitor binding mode. Research for the identification of new lead compounds is mainly driven by the screening of large compound collections, where up to millions of chemical entities form a single library. Because the method presented herein detects direct binding of inhibitors, it does not rely on catalytically active kinase preparations, costly reagents such as kinase substrates, or radioactivity. It may therefore offer an inexpensive alternative to current kinase inhibitor screening methods used by both academia and industry. Ongoing work is focused on adapting this approach to a 384-well format to screen large compound

(39) Weisberg, E.; Manley, P. W.; Breitenstein, W.; Bruggen, J.; Cowan-Jacob, S. W.; Ray, A.; Huntly, B.; Fabbro, D.; Fendrich, G.; Hall-Meyers, E.; Kung, A. L.; Mestan, J.; Daley, G. Q.; Callahan, L.; Catley, L.; Cavazza, C.; Azam, M.; Neuberg, D.; Wright, R. D.; Gilliland, D. G.; Griffin, J. D. *Cancer Cell* **2005**, *7*, 129–41.
(40) Adrian, F. J.; Ding, Q.; Sim, T.; Velentza, A.; Sloan, C.; Liu, Y.; Zhang, G.; Hur, W.; Ding, S.; Manley, P.; Mestan, J.; Fabbro, D.; Gray, N. S. *Nat. Chem. Biol.* **2006**, *2*, 95–102.
(41) Calleja, V.; Laguerre, M.; Parker, P. J.; Larijani, B. *PLoS Biol.* **2009**, *7*, 189–200.
(42) Fischmann, T.; Smith, C.; Mayhood, T.; Myers, J.; Reichert, P.; Mannarino, A.; Carr, D.; Zhu, H.; Wong, J.; Yang, R. S.; Le, H.; Madison, V. *Biochemistry*, doi:10.1021/bi801898e.
(43) Kirkland, L. O.; McInnes, C. *Biochem. Pharmacol.* **2009**, *77*, 1561–71.

libraries. The application of this new assay system to drug targets such as EGFR, Abl, PDGFR, and Kit, as we applied to cSrc kinase,[28] may eventually spur the development of new chemical entities, which take advantage of allosteric binding sites and lead to more specific drugs, some of which may be able to overcome the emerging problem of kinase drug resistance mutations. Its application will be particularly fostered by first answering the question of which kinases can adopt targetable inactive conformations.

Supporting Information Available: Experimental details for the chemical synthesis of the focused library of pyrazolourea-based type II and type III ligands, data collection and refinement statistics for p38α cocrystallized with several ligands, several additional figures, complete refs 10, 12, 26, and 38, as well as further discussions regarding the characterization of p38α conjugated with additional fluorophores, the SAR of type II hybrid inhibitors, and the validation of sorafenib as a potent type II p38α inhibitor. This material is available free of charge via the Internet at http://pubs.acs.org.

JA902010P